BCSJ

# Single-Particle Tracking Reveals a Dynamic Role of Actin Filaments in Assisting Long-Range Axonal Transport in Neurons

**Yasuko Osakada*[1,2] and Kai Zhang[3]**

[1]Department of Chemistry, Stanford University, Stanford, CA 94305 (USA)

[2]The Institute of Scientific and Industrial Research (SANKEN), Osaka University, Mihogaoka 8-1, Ibaraki, Osaka 567-0047

[3]Department of Biochemistry, School of Molecular and Cellular Biology, University of Illinois at Urbana-Champaign, 600 South Mathews Avenue, 314 B Roger Adams Laboratory, Urbana, Illinois, 61801 (USA)

E-mail: yasuko.osakada@gmail.com

Received: March 11, 2017; Accepted: March 24, 2017; Web Released: March 29, 2017

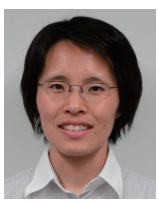

**Yasuko Osakada**

Dr. Yasuko Osakada completed her doctoral work at Osaka University in 2009, under the guidance of Prof. Tetsuro Majima and Prof. Kiyohiko Kawai, where she studied nucleic acid photochemistry. After her experience as a postdoctoral fellow at Stanford university with Prof. Bianxiao Cui and as an assistant professor at Kyoto University with Prof. Yoshie Harada, she was appointed as an assistant professor at The Institute of Scientific and Industrial Research (SANKEN), Osaka University in 2014 and as an associate professor at Institute for Advanced Co-Creation Studies and SANKEN, Osaka University in 2017. Her current interests lie in creating novel materials and methods to examine and regulate biological phenomena in cells, based on principles of photochemistry.

## Abstract

Here, we demonstrated that actin filaments mediate axonal transport in dorsal root ganglia (DRG) neurons using fluorescence single-particle tracking. We employed a compartmentalized microfluidic cell culturing chamber that allows depolymerization of actin filaments within an axonal segment. We observed that local actin depolymerization results in a two-fold increase in the average pausing duration, whereas the microtubule-dependent instantaneous transport speed is not perturbed. Collectively, our data reveal an important role of actin filaments in assisting microtubule-dependent long-range NGF axonal transport in DRG neurons.

## 1. Introduction

Single-molecule imaging is a powerful tool to observe dynamic behavior in materials science[1,2] and biology. In particular, biological imaging advanced the understanding of cellular structure and dynamics.[3–7] While cellular structures in fixed cells have been imaged by using localization microscopy such as stimulated emission depletion microscopy, reversible saturable optical linear fluorescence transitions microscopy, photoactivated localization microscopy, etc.,[8–10] further examination would be beneficial toward understanding their dynamic events in living cells. Fluorescence single-particle tracking has been increasingly used to track dynamic cellular events. By labeling molecular targets with organic fluorophores[11] or quantum dots (QDs),[12–16] fluorescence single-particle tracking is particularly suitable for studying the trafficking of macromolecules and organelles in living cells.

Normal functionality of highly polarized neuronal cells requires axonal transport of macromolecules such as proteins, mRNAs and organelles.[17,18] The axonal transport machinery is driven by motor proteins to ensure the survival and maintenance of nerve cells.[19] Misregulation in axonal transport has been reported in a variety of neurodegenerative diseases.[20] Thus, understanding of molecular mechanisms by which axonal transport is regulated would shed light on pathological mechanisms of neurodegenerative disorders.[21,22]

Long-range axonal transport in neurons is driven by motor proteins such as kinesins and dyneins that run on microtubule cytoskeletal tracks.[23,24] Together with the microtubule-based movements, actin filaments and their associated motor proteins also contribute to the axonal transport process.[23,25–30] Previous studies, however, have proposed inconsistent models that actin filaments either assist or inhibit axonal transport of organelles. Such inconsistency may arise from experimental procedures that cause global disruptions of actin filaments, which may inadvertently affect other essential cellular functions. In this study, we aim to determine how local disruption of actin filaments affects axonal transport.

We have previously demonstrated single-particle tracking of axonal transport of QDs-labeled nerve growth factor (NGF) in

dorsal root ganglia (DRG) neurons.[31] Retrograde NGF transport displays characteristic stop-and-go patterns that are shared by many organelles moving in the axon.[32–35] However, molecular mechanisms that regulate the frequency and duration of pauses, or those that transiently halt the movement, are still poorly understood. Herein, we aim to determine the role of actin filaments on the kinetics of NGF retrograde transport. Our results suggest that the polymerization states of actin filaments play an important role in regulating long-range NGF transport via modulating endosomal pausing in DRG neurons.

## 2. Experimental

**Chemicals and Reagents.** Polydimethylsiloxane (PDMS) composed of silicone elastomer and curing agent (Sylgard 184 elastomer kit, Dow Corning, Corning, NY) was purchased from Fisher Scientific (Pittsburgh, PA). Poly-L-Lysine (PLL, molecular weight 70,000–150,000), boric acid, sodium tetraborate, methylcellulose, trichloromethyl silane (TCMS), latrunculin B (LatB), monoclonal anti-alpha-tubulin-FITC antibody (cloneDM1A), and BSA were purchased from Sigma-Aldrich Chemical Co. (St. Louis, MO). Modified Eagle's medium (DMEM), and fetal bovine serum (FBS) were purchased from Mediatech Inc. (Herndon, VA). Trypsin 1×, 0.25% in HBSS w/o $Ca^{2+}$ and $Mg^{2+}$ was purchased from cellgro (Manassas, VA). Neurobasal medium, B27, GlutaMAX, hibernate medium, streptavidin-coated QD (605 nm) and Alexa Fluor 568-conjugated phalloidin were purchased from Invitrogen (Carlsbad, CA). Paraformaldehyde was purchased from TCI America (Portland, OR). Cytochalasin D (CD) and cover glasses (24 × 40 $mm^2$, No. 1.5 thickness) were purchased from VWR (West Chester, PA). Detergent (Alconox® Powder Detergent) was purchased from Thermo Fisher. Sprague-Dawley fetal rats were purchased from Charles River (Wilmington, MA).

**Fabrication of PDMS Microfluidic Chips.** A silicon wafer with masks of microfluidic patterns was treated with TCMS vapor for 1 min to facilitate removal of PDMS from the wafer after curing. The silicon wafer was placed on aluminum foil and placed on a 4-inch petri dish. About 40 g of fully mixed silicone elastomer and curing agent (weight ratio, 10:1) were poured onto the silicon wafer. The petri dish was placed in a vacuum chamber and degassed under vacuum for 20 min until no air bubbles appeared. After curing at 60 °C overnight, the PDMS layer was peeled off from the master mold and cut into chips 25 × 15 $mm^2$. Two 7-mm-diameter holes and two 3-mm-diameter holes were punched in each PDMS chip (Figure 1a). PDMS chips were cleaned with detergent, water, ethanol, and sterilized by autoclaving. Glass cover slips were cleaned with detergent, DI water, and ethanol. After cleaning, the glass cover slips were coated with 0.1 mg/mL PLL, washed twice in water, and dried in a sterilized biosafety cabinet. PDMS microfluidic devices were assembled by gently placing a PDMS chip onto a PLL coated cover slip before plating DRG neurons.

**Culturing DRG Neurons.** All animal experiments were performed with the approval of the animal experiment ethics committee at Stanford University and according to the NIH guidelines for the care and use of laboratory animals. Primary embryonic rat dorsal root ganglia neurons were isolated from

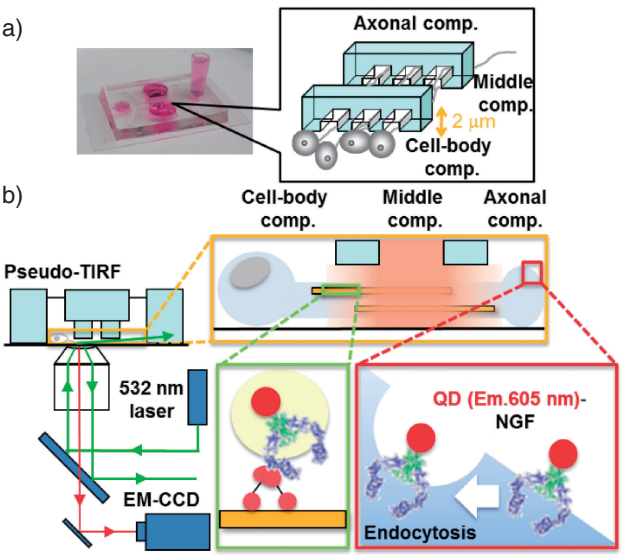


**Figure 1.** (a) Photograph and schematic diagram of DRG culture in the PDMS perfusion chamber. The perfusion chamber is composed of three fluidic compartments (middle, cell-body and axonal compartments) separated by a column of 150 mm long microchannels. DRGs were plated in the cell-body compartment and their axons grew across the channels toward the axonal compartment. The device used in this study is composed of three fluidic compartments (middle, cell-body and axonal compartments) separated by a column of 150 μm long microchannels. The middle compartment of the three-compartment device is about 200 μm wide and can be independently accessed through two small holes. The height of the microchannels (~2 μm) is smaller than the size of a cell-body so that neurons cannot cross from the cell-body compartment to the adjacent compartment during the plating process, but the microchannels are wide enough to permit axons to grow across microchannels. (b) Microfluidic perfusion device for tracking NGF retrograde axonal transport in DRG neurons by TIRF microscope. Side view of microfluidic perfusion microfluidic device. Drugs were perfused in the middle compartments and microchannels with positive pressure. QD (emission; 605 nm)-NGF was tracked under a TIRF microscope to probe the effects of local perfusion of drugs in axonal segments.

Sprague-Dawley fetal rats (age E15–E16). Briefly, dorsal ganglia of rat embryos were collected in 10 mM HEPES in HBSS solution with 200 U/mL penicillin and 200 μg/mL streptomycin. Ganglia cells were enzymatically treated in 0.25% trypsin for 20 min at 37 °C and gently triturated with a 1 mL pipette. DMEM containing 15% FBS was added and cells were spun down to the bottom of the collecting tube. Dissociated DRG neurons were re-suspended in neurobasal medium supplemented with 1× of B27, 2 mM GlutaMAX, 200 U/mL penicillin and 200 μg/mL streptomycin, and 50 ng/mL NGF (maintenance medium). Cell density was counted by a hemacytometer and 10 μL cell suspension ($10^5$ cells/mL) was seeded into each chamber. After 10 min of cell plating, maintenance medium was added to one 7-mm-diameter hole and one 3-mm-diameter hole, respectively. All cultures were housed in a humidified


 

incubator at 37 °C supplied with 5% $CO_2$. Two days after plating, 4 μM cytosine arabinoside (1-β-D-arabinofuranosylcytosine) was added to every hole and was incubated for 15 h to suppress growth of non-neuronal cells. Three hours prior to imaging, 2 nM QD-NGF was added to the axonal compartment of the perfusion chamber. NGF was purified from mouse submaxillary glands, biotinylated and coupled to QD via biotin-streptavidin interaction.[31]

**Drug Perfusion Experiments.** A 200 μL pipette tip was truncated to one inch length and was inserted into a hole in the middle compartment. Drug solution was added into the pipette tip. To facilitate drug perfusion, liquid was removed from the other 3-mm-diameter hole. To visualize the effect of perfusion, we added 2 μM of acridin orange in the middle opening pipette and imaged with a fluorescent microscope (Leica 2000M). Fluorescence intensities were quantified by averaging signal from each compartment from 10 images.

**Immunostaining.** DRG neurons were fixed with 4% paraformaldehyde (for actin) or, 3% paraformaldehyde and 0.1% glutaraldehyde (for microtubule) in PBS for 20 min and washed with PBS. After the fixation, 20, 40, 60, 80 and 100% methanol in milliQ water were added sequentially and PDMS was removed from the cover slide. Next, the cells were incubated in BSA solution for 60 min, stained with phalloidin-Alex 568 dye or anti-tubuline FITC for 60 min, and washed twice with PBS and in water (5 min each). Anti-fade solution was used to mount the thin cover slip on the cover slide. The edge of the cover slip was then sealed with nail polish. Cells were imaged under a Leica fluorescent microscope with a 100× N.A. oil immersion objective.

**Pseudo Total Internal Reflection Fluorescence (TIRF) Imaging.** An inverted Nikon microscope (Ti-U) was modified for pseudo-TIRF illumination. The 532-nm laser beam (Spectra-Physics) was expanded to 3 cm in diameter and then focused at the back focal plane of the objective lens (TIRF 60×, *N.A.* 1.49, Nikon). The focal point was moved off-axis so that the light underwent total internal reflection at the glass–water interface. The angle of refraction was then carefully tuned by moving the focusing lens that was mounted on a translation stage. The incident angle was adjusted to be slightly smaller than the critical angle so that the laser beam could penetrate 1 mm into the aqueous solution. Three hours prior to imaging, 2 nM NGF-QD was supplied in the axonal compartment of the microfluidic chamber. Immediately before imaging, the microfluidic chamber was transferred from the incubator to a customized microscope stage, pre-warmed to 37 °C. Free NGF-QD in solution was then washed off and the culture medium was replaced by hibernate medium supplemented with B27. Fluorescence emission from the QD was collected by the objective lens, transmitted through the 625DCLP dichroic mirror, filtered with a QD605/20 emission filter (Chroma Technology, Rockingham, VT) and focused onto a sensitive EMCCD CCD camera (Andor, South Windsor, CT). Time-lapsed images were collected at a speed of 10 frames/s. A home-made temperature control system was used to regulate the temperature of both the microscope stage and the objective.

**Data Analysis.** Fluorescently labeled endosomes were identified as the local maxima with a signal-to-noise ratio larger than 3 after background subtraction. Spatial distribution of the fluorescence intensity of individual endosomes was fitted with a two-dimensional Gaussian function. The fitted center, corresponding to the position of the endosome, was located with a precision of 10 nm. After measuring the position of endosomes at consecutively timed images, the positions were plotted with time to construct a kymograph. The average speed was determined by measuring the distance of endosome travel over the observation time. Pausing duration was determined by summing all static segments along the kymograph over the total data acquisition time.

## 3. Results and Discussion

To examine the effect of locally disrupted actin filaments on NGF axonal transport in DRG neurons, we first designed a three-compartment microfluidic perfusion chamber that permits local administration of drugs (Figure 1a).[18,36,37] In brief, the middle compartment can be accessed by two small holes that are connected to the cell-body and axonal compartments via microchannels (Figures 1a and 1b). Drug was loaded from one hole through a pipette tip (Figure S1a). The device for DRG neurons was fabricated using soft-lithography as previously described (Figure S1).[31] We then examined the local delivery of small-molecule drugs and their effects on actin dynamics (Figures S2–S5). We used immunostaining to probe local depolymerization of actin filaments in DRG neurons induced by latrunculin B (LatB) and cytochalasin D (CD). LatB and CD are commonly used reagents that inhibit actin polymerization.[25,26] Fluorescence intensity of immuno-stained actin filaments was significantly diminished in the microchannels upon LatB (2 μM) or CD (20 μM) perfusion, compared with that of non-treated neurons (control) (Figure S3).

On the other hand, fluorescence intensity did not change in the cell-body and axonal compartments (Figure S4). These results suggest that treatment with LatB or CD locally depolymerized actin filaments, in the microchannels and middle compartments. In comparison, we also stained the microtubule with FITC-conjugated anti-α-tubulin antibody to examine the microtubule morphology. We did not observe significant changes of microtubules in the microchannels or middle compartment after LatB and CD treatment (Figure S5).

To determine how the polymerization states of actin filaments affect the retrograde transport of NGF in axons, we used real-time imaging to visualize axonal transport at the single-endosome level.[31,34] NGF-biotin was conjugated with streptavidin-coated quantum dots (NGF-QD). NGF retrograde transport was then tracked with a total internal reflection fluorescence (TIRF) microscope equipped with a green laser (532 nm). The speed and pattern of axonal transport were quantified by kymograph analysis (Figure S6 and Supplementary Information). Upon LatB and CD perfusion, the characteristic stop-and-go moving patterns were also observed (Figure S6).[31,33,34]

To quantify patterns of axonal transport, we first analyzed the average speed of transport that includes endosomal pausing (Figure 2 for LatB and S7 for CD). Prior to drug treatment, the basal transport speed was determined based on time-stamped images from NGF-QD transported in microchannels. After drug perfusion, the speed was measured again from the same culture. A 20-min LatB treatment decreased the average speed of NGF retrograde transport by 20% (Figure 2a). After 60

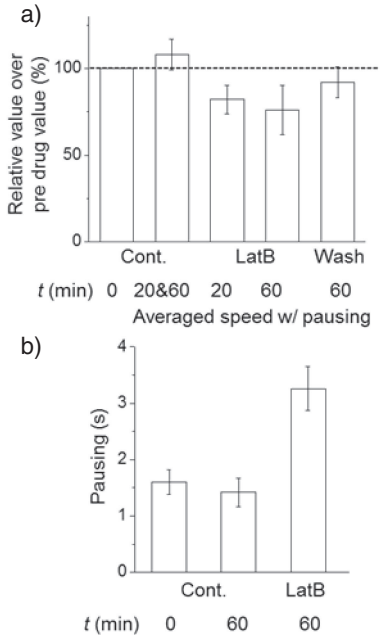


**Figure 2.** (a, b) Effects of LatB-induced actin depolymerization on NGF retrograde axonal transport. (a) Averaged transport speeds that include pausing. The speeds after drug treatment were compared with the speed of pre-drug treatment (at 0 min) in each device. Without drug perfusion (cont., DMSO medium), LatB perfusion for 20 and 60 min without washing, and the speed with 20 min LatB perfusion and washing LatB out at 20 min. (b) Averaged pausing duration for drug perfusion of LatB, respectively. Each value was determined from three independent experiments.

min treatment with LatB, we observed an approximately 25% decrease, compared with the basal level (Figure 2a). The same tendency of reduced speed was also observed when another actin polymerization inhibitor, CD, was applied to the reservoir (~15% reduction after 20 min and ~20% after 60 min, Figure S7a). With the control medium, the slight increase of speed (approximately 10%) observed was probably due to the recovery of neurons from the condition change. Our results showed that depolymerization of actin filaments by LatB or CD reduced the rate of NGF-QD retrograde axonal transport. In addition, the decreased transport rate, induced by the depletion of actin filaments, was recovered back to approximately 90%, by washing out LatB from the reservoir after 20 min of LatB treatment, followed by a recovery for another 40 min (Figure 2a, "wash"). This result indicates that effect of actin depolymerization on axonal transport is transient and recoverable, because the process of actin polymerization is dynamic and the newly re-polymerized actin filaments are likely to recover their role in the axonal transport process.

Next, we compared the pausing durations before and after drug treatment (Figure 3). We define pausing as periods with a velocity less than 0.1 μm/s in the retrograde direction. We parsed the transport trajectories into active moving and pausing periods, and analyzed each period separately. The instantaneous moving speeds (without pausing) were almost the same as the pre-drug treatment values for each condition (control, LatB and CD perfusion, Figures 3, S7b and S8), suggesting that microtubule-dependent long-range transport is not perturbed by actin depolymerization. These results imply that actin-depolymerization-mediated decrease of axonal transport speed primarily arises from an extension of pausing during transport.

To confirm the above hypothesis, we quantified the pausing durations under each condition (Figures 2b, S7b and S8c). The

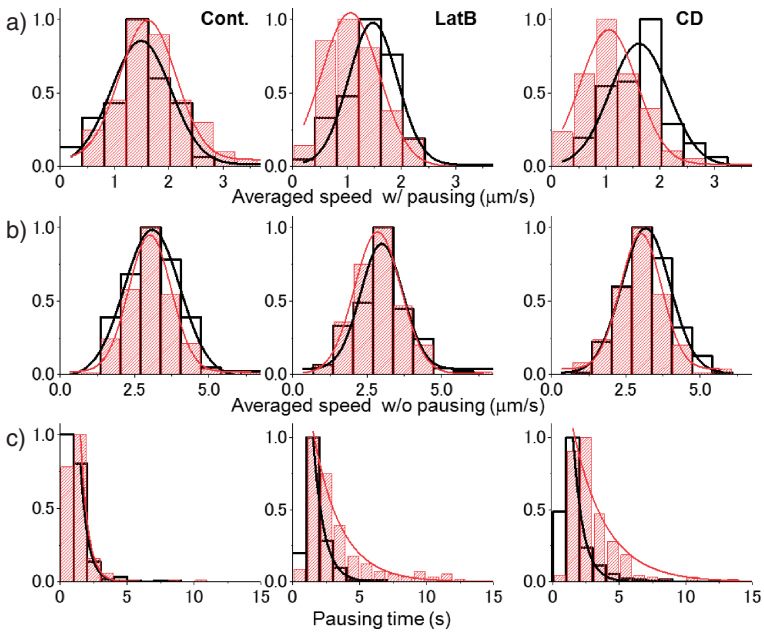


**Figure 3.** (a–c) Representative histograms of averaged speed and pausing time under LatB and CD perfusion. (a) Histograms of averaged speed with pausing duration. (b) Histograms of averaged speed without pausing duration. The histogram was fitted with Gaussian distribution. (c) Histograms of pausing time. The histogram was fitted with single exponential decay. Black bars and curves: prior to drug perfusion; red bars and curves: after drug perfusion. Left; control, middle LatB perfusion for 60 min, right; CD perfusion for 60 min.


 

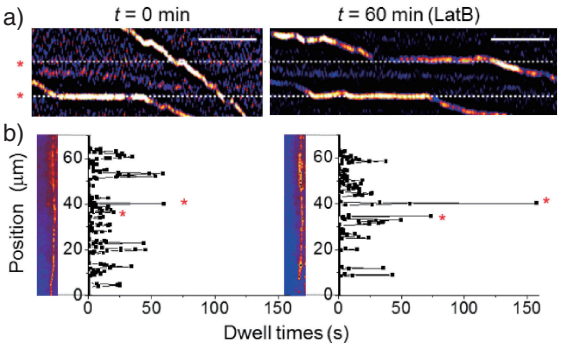


**Figure 4.** Effect of local actin depolymerization in the same axon. (a) Representative kymograph of single endosome travel in the single axon. Left; Pre-drug treatment (control), right; LatB perfusion for 60 min. Scale bar shows 5 s. To observe axonal transport in the same axon, the microfluidic chamber was kept on the microscope stage during drug perfusion. (b) Histogram of pausing dwell time in single axon. Left; prior-drug treatment, right; LatB perfusion for 60 min. Each data were from 5 independent movies. Asterisks show the same positions in the axon in (a). Images are the z-projections of a single axon.

averaged pausing durations under LatB and CD perfusion were about two-fold longer than that of the control (Figure 2b and Table S1). Changes of average transport speed and prolonged pausing mediated by actin depolymerization can be quantified by comparing histograms of the transport speed (Figures 3a–3b) and pausing times (Figure 3c). These results show that actin depolymerization increased the pausing time, indicating that actin filaments assist axonal transport during the pausing process by shortening the waiting time between the active movement in the axonal transport.[23,30,38,39]

In order to determine whether actin depolymerization alters the transport patterns at a specific cellular localization, we measured NGF transport in the same axon before and after LatB perfusion (Figure 4). Five trajectories in a single axon were recorded before LatB perfusion treatment. Another 5 trajectories passing through the same axonal segments were the recorder, 60 min after LatB perfusion. Representative kymographs are shown in Figure 4a. The corresponding z-projection images of NGF-QDs, which outlines the axon profile, are also shown in Figure 4b. Consistent with representative kymographs shown in Figure 4a, endosomes paused at the same place before and after LatB treatment at specific locations, despite the fact that those endosomes were taken 60 min apart (as indicated by the asterisk in Figure 4b). Mechanistic study of correlation between pausing locations and microtubule structures requires probing both cargos and microtubules with high-resolution imaging approaches such as super-resolution microscopy or electron microscopy.[40] These studies are beyond the scope of this study.

## 4. Conclusion

In this study, we investigated the effect of actin filaments on NGF retrograde transport using single-particle tracking in living DRG neurons. Local actin depolymerization slows down endosomes primarily through increasing the pausing duration. While we successfully identified the involvement of local actin dynamics for NGF transport, further examination of transport of other organelles[19,41–43] and the involvement of actin related motors[38,39] will be necessary to comprehend the mechanism of axonal transport more deeply.

Y.O. was supported by Japan Society for the Promotion of Science fellowships for research abroad. K.Z. was supported by the University of Illinois at Urbana-Champaign. We thank Prof. Bianxiao Cui at Stanford University for her support and guidance.

## Supporting Information

This material is available on http://dx.doi.org/10.1246/bcsj.20170090.

## References

1 J. D. Ng, S. P. Upadhyay, A. N. Marquard, K. M. Lupo, D. A. Hinton, N. A. Padilla, D. M. Bates, R. H. Goldsmith, *J. Am. Chem. Soc.* **2016**, *138*, 3876.
2 A. Aloi, A. V. Jentzsch, N. Vilanova, L. Albertazzi, E. W. Meijer, I. K. Voets, *J. Am. Chem. Soc.* **2016**, *138*, 2953.
3 J. Yoo, T.-S. Lee, B. Choi, M. J. Shon, T.-Y. Yoon, *J. Am. Chem. Soc.* **2016**, *138*, 14238.
4 D. K. Sasmal, R. Yadav, H. P. Lu, *J. Am. Chem. Soc.* **2016**, *138*, 8789.
5 V. Glembockyte, R. Lincoln, G. Cosa, *J. Am. Chem. Soc.* **2015**, *137*, 1116.
6 A. T. Bademosi, E. Lauwers, P. Padmanabhan, L. Odierna, Y. J. Chai, A. Papadopulos, G. J. Goodhill, P. Verstreken, B. van Swinderen, F. A. Meunier, *Nat. Commun.* **2017**, *8*, 13660.
7 S. B. Mehta, M. McQuilken, P. J. La Riviere, P. Occhipinti, A. Verma, R. Oldenbourg, A. S. Gladfelter, T. Tani, *Proc. Natl. Acad. Sci. U.S.A.* **2016**, *113*, E6352.
8 H. Deschout, F. C. Zanacchi, M. Mlodzianoski, A. Diaspro, J. Bewersdorf, S. T. Hess, K. Braeckmans, *Nat. Methods* **2014**, *11*, 253.
9 U. Endesfelder, M. Heilemann, *Nat. Methods* **2014**, *11*, 235.
10 A. Small, S. Stahlheber, *Nat. Methods* **2014**, *11*, 267.
11 J. B. Grimm, B. P. English, H. Choi, A. K. Muthusamy, B. P. Mehl, P. Dong, T. A. Brown, J. Lippincott-Schwartz, Z. Liu, T. Lionnet, L. D. Lavis, *Nat. Methods* **2016**, *13*, 985.
12 S. Burov, P. Figliozzi, B. Lin, S. A. Rice, N. F. Scherer, A. R. Dinner, *Proc. Natl. Acad. Sci. U.S.A.* **2017**, *114*, 221.
13 H. Li, S.-X. Dou, Y.-R. Liu, W. Li, P. Xie, W.-C. Wang, P.-Y. Wang, *J. Am. Chem. Soc.* **2015**, *137*, 436.
14 S. Saurabh, L. E. Beck, S. Maji, C. J. Baty, Y. Wang, Q. Yan, S. C. Watkins, M. P. Bruchez, *ACS Nano* **2014**, *8*, 11138.
15 E. M. Petrini, T. Ravasenga, T. J. Hausrat, G. Iurilli, U. Olcese, V. Racine, J.-B. Sibarita, T. C. Jacob, S. J. Moss, F. Benfenati, P. Medini, M. Kneussel, A. Barberis, *Nat. Commun.* **2014**, *5*, 3921.
16 B. Biermann, S. Sokoll, J. Klueva, M. Missler, J. S. Wiegert, J.-B. Sibarita, M. Heine, *Nat. Commun.* **2014**, *5*, 3024.
17 J. W. Park, B. Vahidi, A. M. Taylor, S. W. Rhee, N. L. Jeon, *Nat. Protoc.* **2006**, *1*, 2128.
18 A. M. Taylor, D. C. Dieterich, H. T. Ito, S. A. Kim, E. M. Schuman, *Neuron* **2010**, *66*, 57.
19 S. R. Chada, P. J. Hollenbeck, *Curr. Biol.* **2004**, *14*, 1272.
20 L. M. Ittner, T. Fath, Y. D. Ke, M. Bi, J. van Eersel, K. M. Li, P. Gunning, J. Götz, *Proc. Natl. Acad. Sci. U.S.A.* **2008**, *105*,

15997.
21 M. P. Mattson, M. Gleichmann, A. Cheng, *Neuron* **2008**, *60*, 748.
22 T. Tani, Y. Miyamoto, K. E. Fujimori, T. Taguchi, T. Yanagida, Y. Sako, Y. Harada, *J. Neurosci.* **2005**, *25*, 2181.
23 K. A. Myers, Y. He, T. P. Hasaka, P. W. Baas, *Neuroscientist* **2006**, *12*, 107.
24 R. S. B. Williams, L. Cheng, A. W. Mudge, A. J. Harwood, *Nature* **2002**, *417*, 292.
25 R. L. Morris, P. J. Hollenbeck, *J. Cell Biol.* **1995**, *131*, 1315.
26 S. Roy, M. J. Winton, M. M. Black, J. Q. Trojanowski, V. M.-Y. Lee, *J. Neurosci.* **2008**, *28*, 5248.
27 A. J. Reynolds, I. A. Hendry, *Brain Res. Protoc.* **1999**, *3*, 308.
28 T. P. Hasaka, K. A. Myers, P. W. Baas, *J. Neurosci.* **2004**, *24*, 11291.
29 P. C. Bridgman, *Cell Biology of the Axon*, Springer, **2009**, Vol. 48, p. 191. doi:10.1007/400_2009_10.
30 P. W. Baas, C. V. Nadar, K. A. Myers, *Traffic* **2006**, *7*, 490.
31 K. Zhang, Y. Osakada, M. Vrljic, L. Chen, H. V. Mudrakola, B. Cui, *Lab Chip* **2010**, *10*, 2566.
32 B. Cui, C. Wu, L. Chen, A. Ramirez, E. L. Bearer, W.-P. Li, W. C. Mobley, S. Chu, *Proc. Natl. Acad. Sci. U.S.A.* **2007**, *104*, 13666.
33 H. V. Mudrakola, K. Zhang, B. Cui, *Structure* **2009**, *17*, 1433.
34 Y. Osakada, B. Cui, *Methods Mol. Biol.* **2010**, *670*, 231.
35 K. Zhang, P. D. Chowdary, B. Cui, *Methods Mol. Biol.* **2015**, *1298*, 319.
36 S. Takayama, E. Ostuni, P. LeDuc, K. Naruse, D. E. Ingber, G. M. Whitesides, *Nature* **2001**, *411*, 1016.
37 S. Takayama, E. Ostuni, P. LeDuc, K. Naruse, D. E. Ingber, G. M. Whitesides, *Cell Chem. Biol.* **2003**, *10*, 123.
38 D. Pathak, K. J. Sepp, P. J. Hollenbeck, *J. Neurosci.* **2010**, *30*, 8984.
39 N. H. Alami, P. Jung, A. Brown, *J. Neurosci.* **2009**, *29*, 6625.
40 Š. Bálint, I. V. Vilanova, A. S. Alvarez, M. Lakadamyali, *Proc. Natl. Acad. Sci. U.S.A.* **2013**, *110*, 3375.
41 P. J. Hollenbeck, W. M. Saxton, *J. Cell Sci.* **2005**, *118*, 5411.
42 A. Kaasik, D. Safiulina, V. Choubey, M. Kuum, A. Zharkovsky, V. Veksler, *J. Biol. Chem.* **2007**, *282*, 32821.
43 J. Verburg, P. J. Hollenbeck, *J. Neurosci.* **2008**, *28*, 8306.


 